Low-Temperature Fabrication of Wafer-Bonded Ge/Si p-i-n Photodiodes by Layer Exfoliation and Nanosecond-Pulse Laser Annealing

Shaoying Ke, Yujie Ye, Jinyong Wu, Dongxue Liang, Buwen Cheng, Zhiyong Li, Yujiao Ruan, Xiaoying Zhang, Wei Huang, Jianyuan Wang, Jianfang Xu, Cheng Li, and Songyan Chen

***Abstract*— We report a potential method for the fabrication of Si-based Ge film with low threading dislocation (TD) density ($<10^5$ cm^{-2}) based on a low-temperature Ge/Si wafer bonding and smart cut technique. This method may replace the traditional epitaxial growth to solve the problems related to the TDs, high temperature, and high vacuum. A near-bubble-free Ge/Si bonded interface is achieved for the fabrication of Ge/Si p-i-n photodiodes. The insertion of amorphous Ge (a-Ge) has crystallized after Ge layer exfoliation, achieving a small $FWHM_{XRD}$ (96 arcsec) of the Ge peak. This determines the low dark current density (5.97 mA/cm^2) and low ideality factor (1.19) of the Ge/Si p-i-n photodiode. The exfoliated Ge film suffers from in-plane compression strain due to the expansion of the H_2 gas during the blistering process. Interestingly, the in-plane compression strain turns into tensile strain after high-temperature postannealing due to the faster shrinkage rate of Ge during cooling. The in-plane tensile strain leads to the increase in the responsivity of the photodiode. The responsivity of the photodiode at 1310 nm increases from 0.505 to 0.71 A/W and that at 1550 nm increases from 0.244 to 0.524 A/W after postannealing. More importantly, the redshift of the absorption edge of the Ge/Si photodiode (0.1 A/W at 1630 nm) is also observed. This implies that the wafer-bonded Ge/Si p-i-n photodiode can be comparable with the epitaxial one and can be used for optical communication in all wavelength division multiplexing bands, including the *L*-band (1565–1625 nm) and entire *C*-band (1530–1565 nm).**

***Index Terms*— Ge/Si photodiodes, Ge/Si wafer bonding, layer exfoliation, smart cut, threading dislocation (TD).**

I. Introduction

IN THE past few years, silicon (Si)-based germanium (Ge) photoelectric devices have been gained a growing interest due to the fact that they can achieve an excellent infrared light absorption and can be integrated with Si-CMOS technique [1]–[3]. The low-cost nature of these devices provides great potential to be compatible with large-scale modern IC and they are considered to be a substitute of the traditional InGaAs photodiodes [4]–[6]. Previously, the Ge/Si p-i-n photodiode as a typical device was investigated greatly and has achieved outstanding performances [7]–[9].

Nowadays, the fabrication of Ge/Si p-i-n photodiodes is based on the mature and traditional ultrahigh-vacuum (10^{-8} Pa) and high-temperature (600 °C–800 °C) epitaxial technique [10], [11]. However, the drawback of this technique for heterogeneous epitaxy is that high-density threading dislocations (TDs) (10^8–10^9 cm^{-2}) appear in the Si-based Ge film due to the vertical spread of dislocation loops induced by the 4.2% lattice mismatch between Ge and Si materials [12], [13]. In addition, high-temperature cyclic annealing (900 °C) should be conducted to decrease the TD density [14], [15]. The TDs act as the acceptorlike defects (midgap state) in the Ge film [16], [17], leading to the increase in the dark current of the device. Many modified epitaxial methods, such as two-step Ge layer growth [18], [19], Ge/SiGe multiple quantum well segregation [20], graded SiGe buffer layer growth [21], [22], and selective growth [23], [24], were proposed to decrease the TD density. Although the TD density can be significantly decreased (2.1×10^6 cm^{-2}) with graded SiGe buffer layer, a thick SiGe layer (10 μm) should be grown. The two-step Ge layer growth can confine the TDs to a ~100-nm-thick low-temperature Ge layer. As a result, low TD density (~10^7 cm^{-2}) in upper high-temperature Ge layer can be achieved. This method was developed for the selective

Manuscript received December 17, 2018; accepted January 12, 2019. Date of publication January 25, 2019; date of current version February 22, 2019. This work was supported in part by the National Natural Science Foundation of China under Grant 61474081 and Grant 11673019, in part by the Key Project of the National Natural Science Foundation of China under Grant 61534005, in part by the Natural Science Foundation of Fujian Province under Grant 2015D020, in part by the Science and Technology Project of Xiamen City under Grant 3502Z20154091. The review of this paper was arranged by Editor J. Huang. *(Corresponding author: Songyan Chen.)*

S. Ke, Y. Ye, J. Wu, D. Liang, W. Huang, J. Wang, J. Xu, C. Li, and S. Chen are with the Fujian Provincial Key Laboratory of Semiconductors and Applications, Collaborative Innovation Center for Optoelectronic Semiconductors and Efficient Devices, Department of Physics, Xiamen University, Xiamen 361005, China (e-mail: keshaoying2005@163.com; 594049853@qq.com; 995096377@qq.com; 532017401@qq.com; weihuang@xmu.edu.cn; wangjianyuan@xmu.edu.cn; jfxu@xmu.edu.cn; lich@xmu.edu.cn; sychen@xmu.edu.cn).

B. Cheng and Z. Li are with the State Key Laboratory on Integrated Optoelectronics, Institute of Semiconductors, Chinese Academy of Sciences, Beijing 100083, China (e-mail: cbw@semi.ac.cn; lizhy@semi.ac.cn).

Y. Ruan is with the Xiamen Institute of Measurement and Testing, Xiamen 361005, China (e-mail: xiaoyuanbao@126.com).

X. Zhang is with the School of Opto-electronic and Communication Engineering, Fujian Key Laboratory of Optoelectronic Technology and Devices, Xiamen University of Technology, Xiamen 361024, China (e-mail: xyzhang@xmut.edu.cn).

Color versions of one or more of the figures in this paper are available online at http://ieeexplore.ieee.org.

Digital Object Identifier 10.1109/TED.2019.2893273

growth of Ge film in SiO_2 square window. The TD density of $\sim 10^6$ cm^{-2} was achieved after cyclic annealing. How to lower the fabrication temperature and reduce the TD density to below $\sim 10^5$ cm^{-2} is a difficult problem for the heterogeneous epitaxial technique due to the direct contact of the Ge and Si material during epitaxial growth.

Many groups have fabricated Ge/Si p-i-n photodiode based on epitaxial Ge film, the dark current density (DCD) still cannot achieve an expected value. Loh *et al.* [25] reported a selective epitaxial growth of Ge photodiode using low-temperature ultrathin $Si_{0.8}Ge_{0.2}$ buffer layer. The DCD of 27 mA/cm^2 and the low responsivity of 0.037 A/W were achieved. Steglich *et al.* [26] showed an epitaxial Ge/Si photodiode with black silicon light-trapping. Although the responsivity at 1550 nm increases to 0.34 A/W, the DCD of the device is large (150 mA/cm^2). Schmid *et al.* [27] also reported a vertical Ge/Si p-i-n photodiode fabricated by SiGe molecular beam epitaxy. The DCD of 50 mA/cm^2 was achieved and the responsivity at 1550 nm is only $\sim$0.1 A/W. Our group also published a two-step grown Ge/Si photodiode [19], [20]. The responsivity of 0.23 A/W at 1550 nm and the DCD of 10 mA/cm^2 was achieved. Recently, Lin *et al.* [28] reported an interesting work, in which the epitaxial Ge on the initial Si substrate was transferred to a new substrate by wafer bonding technique to eliminate high-density TDs in low-temperature Ge layer. However, the DCD is still limited to $\sim$47 mA/cm^2. Overall, the DCD of the epitaxial p-i-n photodiode is relatively high due to the high density of TDs. This is also a bottleneck for the Ge epitaxial growth at present.

One potential method for further decreasing the TD density is the heterogeneous wafer bonding and smart cut technique. Based on this layer exfoliation technique, we can artificially put a thin amorphous semiconductor material, such as amorphous Si and amorphous Ge (a-Ge), between Ge and Si to avoid the lattice mismatch. This not only can fundamentally eliminate the source of the misfit dislocation but does not affect the carrier transport significantly due to the thin amorphous inserted layer. It should be noted that the introduction of amorphous material cannot be achieved in the epitaxial technique due to the fact that the epitaxial growth should be along the crystal orientation.

Recently, high-quality Ge thin film with several hundred nanometers was exfoliated from bulk Ge and directly bonded with SiO_2 using hydrophilic bonding for the fabrication of Ge-on-insulator [29]–[32]. The H^+ implantation dose is generally larger than 5×10^{16} cm^{-2} and the implantation energy is related to the exfoliated Ge film thickness. The Ge/SiO_2 bonded interface is generally bubble-free due to the fact that the SiO_2 can transfer the by-products (H_2 and H_2O) induced by the hydrophilic reaction at the bonded interface outside the wafer. In addition, the oxide layer formed by the hydrophilic reaction cannot affect the electrical properties of the Ge layer. For Ge/Si wafer bonding, the SiO_2 layer is absent. The bubbles at Ge/Si bonded interface cannot be transferred outside after bonding. More importantly, the hydrophilic oxide at Ge/Si bonded interface may affect the carrier transport of the device. Thus, few works reported on the Ge layer exfoliation on Si wafer and the photodiode based on this technique [33], [34].

In this paper, we combine the low-temperature Ge/Si wafer bonding technique with smart cut technique to exfoliate a high-quality Ge film from bulk Ge on Si substrate. It is important that the Ge/Si bonded interface is demonstrated to be oxide-layer-free and near-bubble-free. Four p-i-n photodiodes are fabricated based on this exfoliated Ge film. In addition, in order to achieve low-temperature conduction through the whole fabrication process, the impurity activation by rapid thermal annealing at 600 °C is replaced by the pulse laser annealing at room temperature. Low DCD of 5.97 mA/cm^2 of the Ge/Si p-i-n photodiode is achieved for 24-μm-diameter mesa. High responsivity of 0.71 A/W at 1310 nm and 0.524 A/W at 1550 nm of our wafer-bonded Ge/Si p-i-n photodiode is also obtained. This indicates that our wafer-bonded photodiode can be comparable with the epitaxial one.

II. Experimental Details

The (001)-oriented n^+-Si substrates ($\sim$0.001 $\Omega \cdot$cm, 2 cm $\times$ 2 cm) and (001)-oriented i-Ge ($>$30 $\Omega \cdot$cm, 2 cm $\times$ 2 cm) substrates were used for Ge/Si wafer bonding. Before bonding, the Ge substrate was ultrasonically cleaned with acetone and alcohol for 10 min, then a 90-nm-thick SiO_2 layer was deposited on the Ge surface by plasma-enhanced chemical vapor deposition to protect the Ge surface during high-energy H^+ implantation. The Ge surface was then implanted at room temperature with H^+ at a dose of 5×10^{16} cm^2 and energy of 150 keV to create a defective blistered region below the Ge surface ($\sim$1.2 μm below Ge surface). After the H^+ implantation, the SiO_2 layer was removed in a dilute hydrofluoric acid solution. All the Si wafers were cleaned with standard RCA process. After cleaning, the Ge and Si wafers were loaded into the dc-magnetron sputtering system to form a thin a-Ge layer ($\sim$2 nm) on the substrate for hydrophilic wafer bonding. Then, the wafers were taken out of the chamber and contacted each other to achieve the prebonding by van der Waals force. Afterward, a set of the Ge/Si wafer pairs were put into a wafer bonder to achieve bonding and layer exfoliation. In order to achieve high bonding strength, promote the lateral diffusion of H_2 gas, and relax the thermal stress between Ge and Si, the multistep annealing is carried out. First, the sample was annealed at 150 °C under a force of 2 MPa for 1 h. Then, the sample was annealed at 250 °C under a force of 0.5 MPa for 1 h. Afterward the sample was annealed at 350 °C without force for 1 h. Finally, 400 °C annealing was conducted for 1 h to trigger the exfoliation of Ge film. The heating rate of 5 °C/min was applied. The whole bonding process was under a chamber pressure of 10^{-5} mbar. Another set of the wafer pairs were bonded in the wafer bonder at 100 °C under a force of 2 MPa for 1 h. Afterward, the Ge/Si wafer pairs were *ex situ* annealed in N_2 atmosphere in tube furnace at a low temperature of 300 °C for 30 h to trigger the exfoliation of the Ge film. For repairing the defects in the exfoliated Ge film, a part of the Ge/Si film was annealed at 500 °C for 1 h. Subsequently, the exfoliated Ge film was polished by chemical mechanical polishing (CMP). Afterward, the Ge film was implanted with BF_2^+ and the impurity was activated by nanosecond pulse laser annealing in N_2 atmosphere to form the

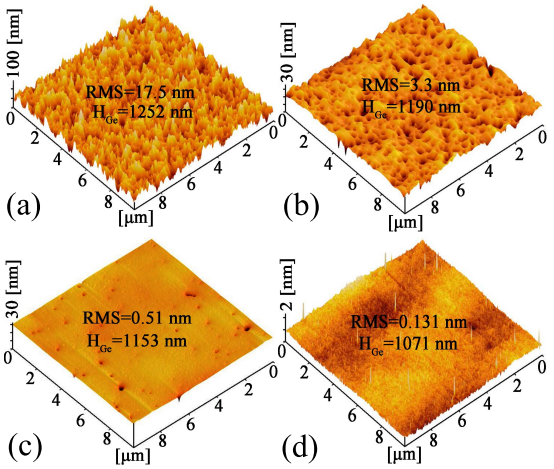

Fig. 1. (a)–(d) AFM images of the exfoliated Ge film polished for 0, 10, 15, and 20 min, respectively.

p^+-Ge layer at room temperature. Finally, the wafer-bonded Ge/Si p-i-n photodiode with different mesas was defined by photolithography.

The a-Ge morphology was examined *ex situ* by atomic force microscope (AFM) and optical microscope. The Ge/Si bonded interfaces were identified by scanning electron microscope (SEM). The bubbles at bonded interfaces were examined by a C-mode scanning acoustic microscope (C-SAM) with a frequency of 250 MHz. The residual in-plane strain and crystal quality of the Ge film were evaluated by double crystal X-ray diffraction (XRD) measurement with 0.15406 nm X-ray source and Raman scattering with 532-nm laser. The secondary ion mass spectroscopy (SIMS) was applied to evaluate the concentration of the doping atoms.

III. Results and Discussion

Here, we name the Ge film exfoliated at 150 °C –400 °C for 1 h as sample (4) and the Ge film exfoliated at 300 °C for 30 h as sample (3). Fig. 1(a)–(d) shows the surface signal of the Ge film in sample (4) after CMP for a different time. We find that the Ge surface is rough (rms = 17.5 nm) after exfoliation [Fig. 1(a)]. This is due to the lateral extension and the burst of the inner H_2 bubbles. When the CMP is conducted for 10 min, the rms of the Ge surface dramatically decreases to 3.3 nm [Fig. 1(b)] and the Ge film thickness decreases to 1.19 μm. When the Ge film is polished for 15 min (or 20 min), the rms further decreases to 0.51 nm (or 0.131 nm). This is enough for the fabrication of photoelectric device. Finally, the Ge film thickness decreases to 1.071 μm after CMP.

The cross section SEM images of sample (4) and sample (3) are shown in Fig. 2(a) and (c), respectively. One can see that the Ge film is uniformly located on the Si substrate. The C-SAM images of these two samples are shown in Fig. 2(b) and (d), respectively. Note that the C-SAM is a sensitive technique to detect the bubbles at the bonded interface and the bubble density is an important parameter to evaluate the quality of the bonded wafer pairs. It is found that the bubble density in sample (4) is much lower than that in sample (3). The interface bubbles originate from the hydrophilic reactions [(1) and (2)] at the bonded interface.

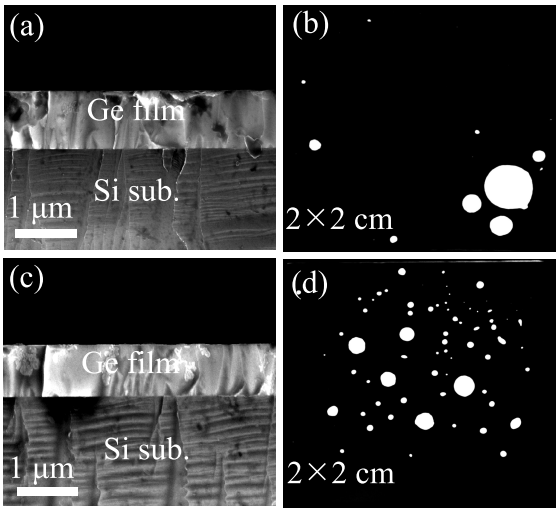

Fig. 2. (a) and (c) SEM images of samples (4) and (3). (b) and (d) C-SAM images of samples (4) and (3).

Thus, it suggests that the lower bubble density in sample (4) is due to the short-time annealing of the wafer pairs in the wafer bonder. Long-time annealing of sample (3) promotes more hydrophilic reactions and produces more H_2 at the bonded interface

$$\mathrm{Ge-OH+OH-Ge \rightarrow Ge-O-Ge+H_2O} \quad (1)$$

$$\mathrm{Ge+2H_2O \rightarrow GeO_2+2H_2}. \quad (2)$$

Fig. 3(a) shows the (004) diffraction peak of sample (3) polished for a different time. The in-plane strain ($\varepsilon_{//}$) in the Ge film is calculated by the equations in [35] and [36]. The positive and negative value of $\varepsilon_{//}$ indicates either tensile or compressive strain. It is noteworthy at this point that the $\varepsilon_{//}$ in the exfoliated Ge film is negative, as shown in Fig. 3(a). This indicates that there is a compression strain in the exfoliated Ge film. This is attributed to the expansion of the H_2-gas bubbles during the blistering process, which implements compressive stress on the lattice surrounding them [32]. With the increase of the polishing time, the in-plane compression strain in the Ge film increases. As mentioned above, the Ge surface is rough after exfoliation. Thus, the surface of the Ge film can be regarded as a damage layer. This damage layer may scatter a part of the X-ray when the examination is conducted. When the CMP is conducted, this damage layer is removed gradually, leading to the left shift of the Ge peak. Fig. 3(b) shows the XRD curves of the exfoliated samples. It is noticeable that the in-plane compression strain in the Ge film of sample (4) (−0.275%) is higher than that of sample (3) (−0.206%) and the full-width at half-maximum (FWHM) of sample (4) (FWHM = 96 arcsec) is smaller than that of sample (3) (FWHM = 122 arcsec). The FWHM of 96 arcsec is much smaller than that of Si-based epitaxial Ge film [19], [20]. When the Ge film is exfoliated by short-time annealing, the interface a-Ge has crystallized and no oxide layer can be observed at the bonded interface, as shown in Fig. 4.

As reported in our previous work [37], [38], when the Ge/Si wafer pairs were annealed at 300 °C for 30 h, the interface a-Ge has also crystallized. The oxide layer also cannot be

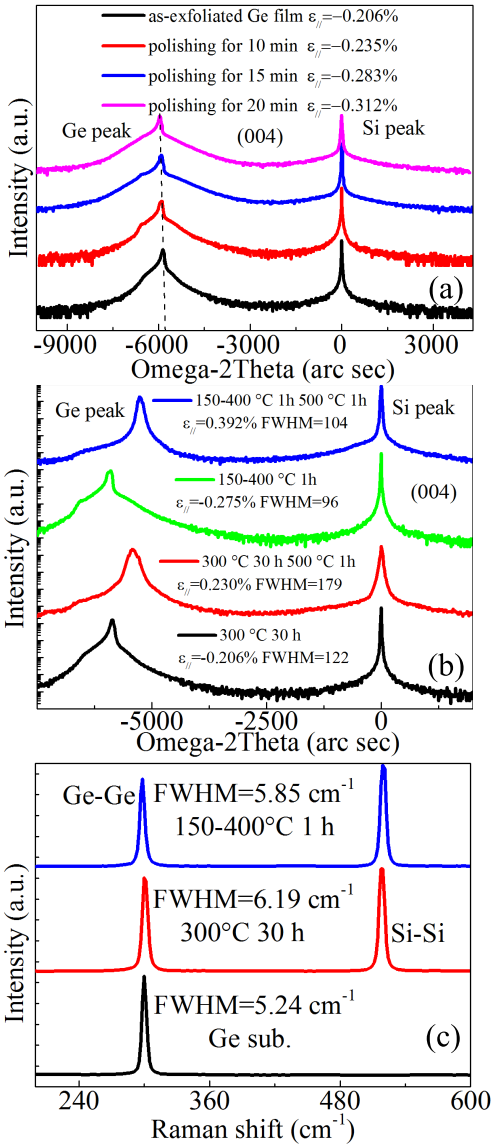

Fig. 3. (a) XRD curves of the samples polished for a different time. (b) XRD curves of the samples annealed at different conditions. (c) Raman spectrum of the exfoliated Ge film.

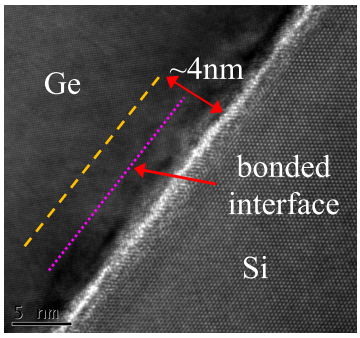

Fig. 4. Cross section TEM image of the Ge/Si bonded interface in sample (4).

observed at the bonded interface. Fig. 3(c) shows the Raman shift of the exfoliated Ge film. One can see that the FWHM of the Ge peak is very close to that of the bulk Ge. This also represents the high quality of our exfoliated Ge film.

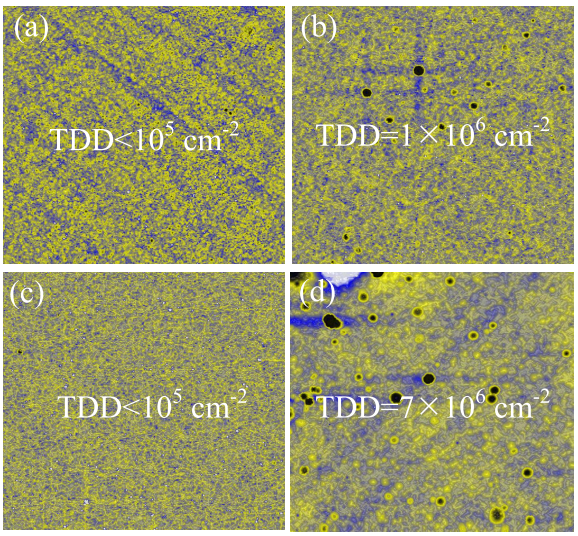

Fig. 5. AFM images (10 μm × 10 μm) of (a) sample (4), (b) sample (45), (c) sample (3), and (d) sample (35) etched by secco solution for 10 s.

Note that the Ge peak, as shown in Fig. 3(b), exhibits a shoulder peak at the left side for exfoliated Ge film. This is due to the interference effects between substrate and strained layers, which are created by the hydrogen implant [30], [32], [39]. In order to relax the nonuniform compressive strain and repair the point defects in Ge layer, the postannealing at 500 °C for 1 h is executed. Here, we name sample (4) further annealed at 500 °C for 1 h as sample (45) and sample (3) further annealed at 500 °C for 1 h as sample (35). One can see that the shoulder peak at the left side of the Ge peak disappears and the Ge peak shows a significant right shift, representing the relaxation of the compressive strain in the Ge film. In addition, after postannealing, the calculated $\varepsilon_{//}$ is positive, indicating the existence of in-plane tensile strain in Ge film. This is attributed to the fact that the Ge shrinks faster than Si during cooling due to the larger coefficient of thermal expansion of Ge [19], [20]. Unfortunately, after postannealing, the FWHM of the Ge peak increases, especially for sample (35) (FWHM = 179). We consider that this feature is ascribed to the introduction of the TDs after annealing.

In order to confirm this hypothesis, the etch pit method using Secco solution [40] is applied to estimate the TD density. As shown in Fig. 5(a) and (c), when the Ge film is exfoliated, the TD density in the Ge film is less than 10^5 cm^{-2}. As shown in Fig. 5(b) and (d), after annealing, the TD density increases to $>10^6$ cm^{-2}. In addition, the TD density in sample (35) (7×10^6 cm^{-2}) is much larger than that in sample (45) (1×10^6 cm^{-2}). This indicates that in Ge/Si wafer bonding system, high-temperature postannealing can lead to the formation of TDs.

In order to achieve a low-temperature activation of doping atoms to form p^+-Ge layer, the nanosecond-pulse laser annealing of the Ge film is carried out. The laser energy, spot size, and pulsewidth of the laser are set to 36 mJ, 3 × 4 cm, and 25 ns, respectively. The annealing process is conducted in the N_2 atmosphere to avoid the oxidation of the Ge surface. The SIMS measurement of the Ge surface is shown in Fig. 6. One can see that the junction depth of the Ge surface is

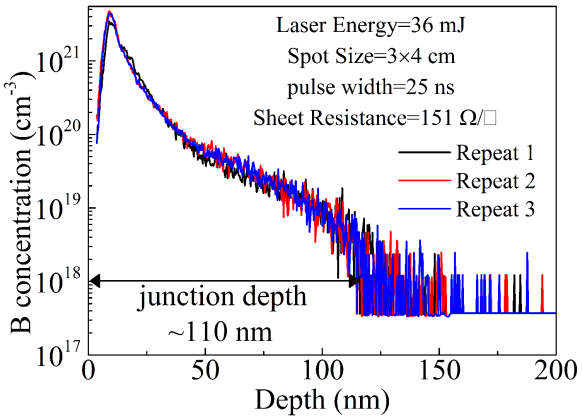

Fig. 6. SIMS measurement of the Ge film after pulse laser annealing.

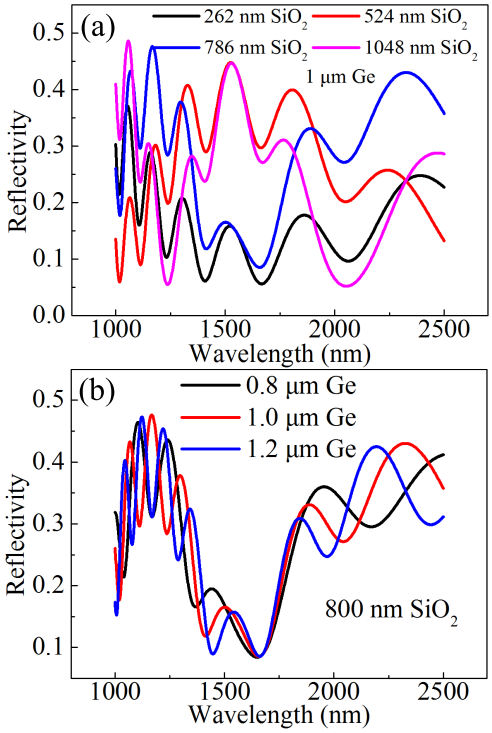

Fig. 7. (a) Effect of SiO_2 thickness on the reflectivity. (b) Effect of Ge layer thickness on the reflectivity.

~110 nm and the sheet resistance of 150 Ω/□ is achieved. We can deduce that the doping concentration of the Ge film is $>10^{19}$ cm^{-3}. This is enough for the achievement of the ohmic contact. For the fabrication of the Ge/Si p-i-n device, the SiO_2 film should be deposited on Ge and Si surfaces to passivate the dangling bonds. It is known that the deposition of SiO_2 also affects the reflectivity of the whole device and the parasitic capacitance of the device. Thus, we simulate the effect of the SiO_2 and Ge layer thickness on the reflectivity of the device, as shown in Fig. 7. One can see from Fig. 7(a) that for the $\lambda/4$ and $3\lambda/4$ thickness (262 and 786 nm) of SiO_2, the device with 1-μm-thick Ge achieves the lowest reflectivity at 1550 nm. The effect of the Ge layer thickness on the reflectivity can be ignored, as shown in Fig. 7(b). In order to achieve a lowest parasitic capacitance between the metal pad and the n^+-Si substrate, the thickness of 786 nm is selected.

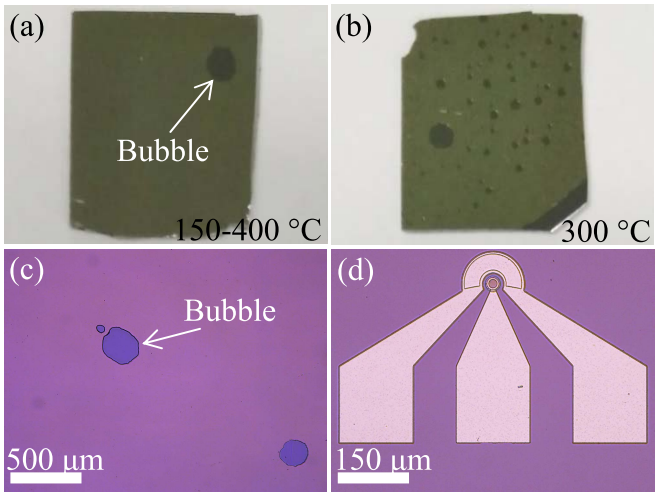

Fig. 8. Camera images of the Ge film in (a) sample (4) and (b) sample (3). Optical microscope images of (a) the exfoliated Ge film and (b) the wafer bonded Ge/Si p-i-n photodetector.

Fig. 8(a) and (b) shows the camera images of the Ge film. One can see that the bubbles at the bonded interface have been burst due to the high pressure of H_2 in the bubbles, exposing the Si substrate to the air. Moreover, few bubbles appear at the bonded interface in sample (4) and some bubbles exist at the bonded interface in sample (3). This result is consistent with the C-SAM images in Fig. 2. The optical microscope images of the exfoliated Ge and the wafer-bonded Ge/Si p-i-n photodiode are shown in Fig. 8(c) and (d), respectively. The mesas with 24, 32, 48, 64, and 100 μm diameter are fabricated.

The I–V curves of different mesas of samples (4) and (3) are shown in Fig. 9(a) and (b). For sample (4), low DCD of 5.97 mA/cm^2 is achieved for 24-μm-diameter mesa at -1 V and that of 14.1 mA/cm^2 is achieved for 32-μm-diameter mesa. This implies that the exfoliated Ge film can achieve low dark current of the device. For sample (3), the DCD is higher than that of sample (4)

$$I = [I_{\text{bulk}} \times (\pi/4)]d^2 + [I_{\text{surface}} \times \pi]d. \tag{3}$$

In order to reveal the source of the leakage current, the dark current and mesa diameter are fitted by (3) to extract the bulk leakage current and the surface leakage current, as shown in Fig. 9(e) and (f). Where I is the total current, I_{bulk} is the bulk leakage current, I_{surf} is the surface leakage, and d is the mesa diameter. One can see that the surface leakage current of these two samples is similar (2.5 μA/cm). This indicates that the Ge sidewall in our sample is well passivated. The bulk leakage current of 45.8 mA/cm^2 is achieved for sample (4), whereas it increases to 132.5 mA/cm^2 for sample (3). This indicates that although the TD density of the two exfoliated samples is lower than 10^5 cm^{-2}, the introduction of the misfit dislocation also affects the dark current of the device. Note that as shown in Fig. 9(c), (d), (g), and (h), when the samples are further annealed at 500 °C for 1 h, the DCD of samples (45) and (35) with 24-μm-diameter mesas increases to 0.387 and 0.724 A/cm^2, respectively. Although the surface leakage current (~2 μA/cm) shows a little change, unfortunately, the bulk leakage current density of these two

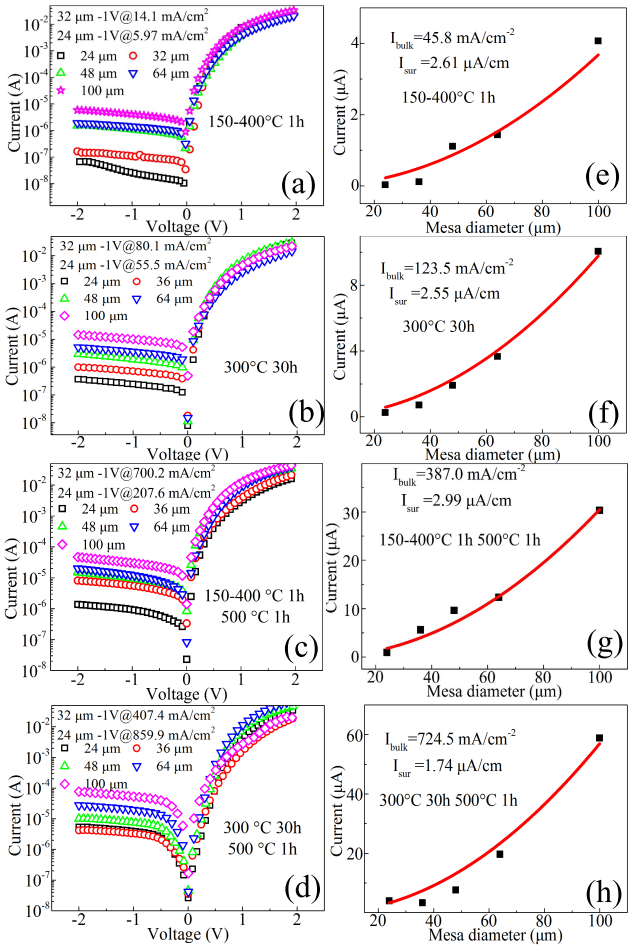

Fig. 9. (a)–(d) *I–V* curves of different mesas of samples (4), (3), (45), and (35). (e)–(h) Current versus mesa diameter for samples (4), (3), (45), and (35).

samples both increases to several A/cm^2 when postannealing is applied. This is ascribed to increase of the TD density after postannealing.

The activation energy of the devices is extracted by (4), as shown in Fig. 10(a)–(d). Where T is the device temperature, E_a is the activation energy, V_a is the applied bias, and k is Boltzmann's constant. One can see that the activation energy of all the samples is close to $E_g/2$ of Ge (0.66 eV) except sample (35). This indicates that the carrier transport in samples (4), (3), and (45) is dominated by the generation/recombination mechanism. This results from the carrier recombination at the defects (point defects in the exfoliated Ge film and the TDs in the postannealed Ge film) in the Ge layer. For sample (35), the activation energy is smaller than $E_g/2$ of Ge. It is believed that some tunneling mechanisms appear in this device due to the higher-density defects in the Ge film

$$I = AT^{3/2}\exp(-E_a/kT)(\exp(qV_a/2kT) - 1). \quad (4)$$

The photocurrent of the devices with 24-μm-diameter mesas illuminated by 1310- and 1550-nm lasers is obtained at room temperature, as shown in Fig. 11. The optical power of the laser is set to 1 mW. We have calibrated this value from the output of the fiber. In principle, the spot size in fiber is 4 μm (diameter). The fiber is adjusted to the position where

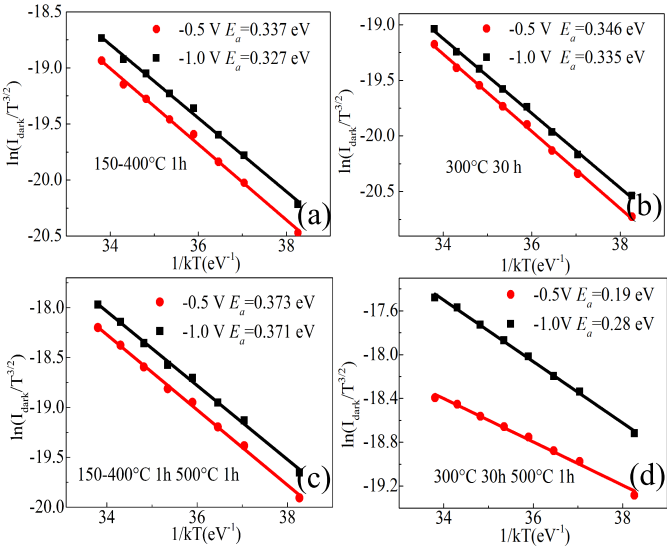

Fig. 10. (a)–(d) Activation energy of samples (4), (3), (45), and (35).

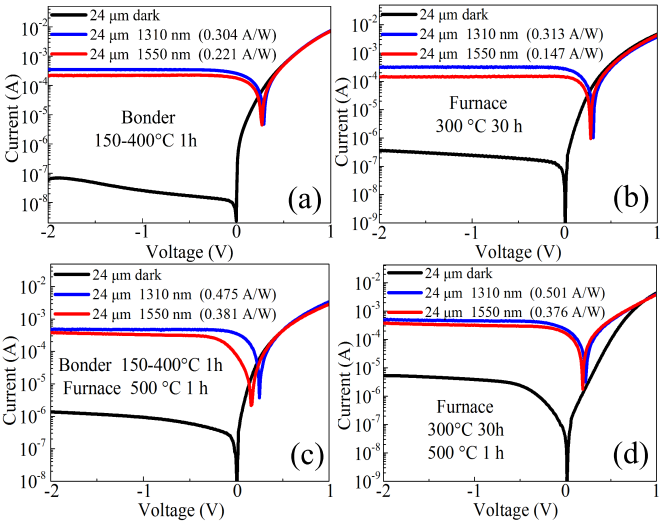

Fig. 11. Photocurrents of (a) sample (4), (b) sample (45), (c) sample (3), and (d) sample (35) with 24-μm-diameter mesa illuminated by 1310- and 1550-nm lasers.

is very close to the incident surface of the detector and it is almost perpendicular to the incident surface of the detector. Finally, by fine adjusting the position of the fiber, we can ensure that the output light intensity is largest. The responsivity of samples (4) and (3) at 1310 nm is 0.304 and 0.313 A/W, respectively, as shown in Fig. 11(a) and (c). The responsivity of sample (4) (0.211 A/W) at 1550 nm is larger than that of sample (3) (0.147A/W). One feature of particular interest is that when the sample is further annealed at 500 °C for 1 h, the responsivity of the devices at 1310 and 1550 nm both increases, as shown in Fig. 11(b) and (d). The responsivity of sample (4) at 1310 and 1550 nm increases to 0.475 and 0.381 A/W, respectively, and that of sample (3) at 1310 and 1550 nm increases to 0.501 and 0.376 A/W, respectively, after postannealing. As mentioned above, the in-plane compression strain in the exfoliated Ge film turns into tensile strain when the Ge film is further annealed at 500 °C for 1 h. The 0.2%–0.4% tensile strain leads to the increase of

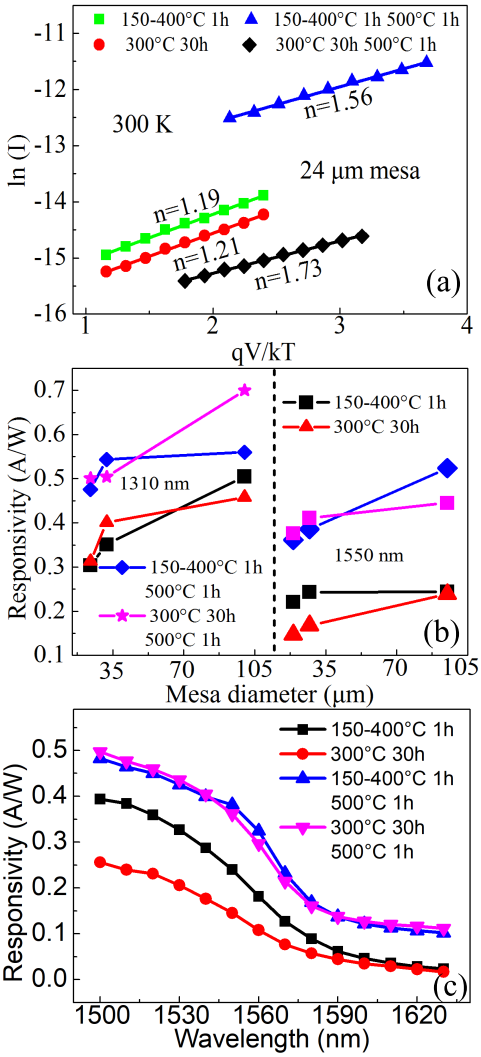

Fig. 12. (a) Ideality factors of the four devices. (b) Responsivity versus mesa diameter at 1310 and 1550 nm. (c) Responsivity versus wavelength.

the absorption of the infrared light, resulting in the increase of the responsivity of the devices.

In order to evaluate the quality of our fabricated wafer-bonded Ge/Si p-i-n photodiodes, the ideality factors of the devices are extracted by (5), as shown in Fig. 12(a). Where I_s is the reverse saturation current and η is the ideality factor. It can see that the lowest ideality factor of 1.19 is achieved for sample (4) and that of 1.21 is achieved for sample (3). This indicates that the quality of our wafer-bonded Ge/Si p-i-n photodiode is nearly ideal. However, for the samples further annealed at 500 °C for 1 h, the ideality factors of samples (45) and (35) increase to 1.56 and 1.73, respectively. This verifies that the sample further annealed at 500 °C for 1 h leads to the deterioration of the device

$$I = I_s \exp(qV_a/\eta kT - 1). \tag{5}$$

The responsivity of the four devices at 1310 and 1550 nm as a function of the mesa diameter is shown in Fig. 12(b). One can see that for 1310-nm wavelength, with the increase of the mesa diameter, the responsivity of the four samples significantly increases. The responsivity of samples (4), (3), (45), and (35) with 100-μm-diameter mesa at 1310 nm is 0.505, 0.458, 0.56, and 0.71 A/W, respectively. For 1550-nm wavelength, the responsivity of the devices also increases with the increase of the mesa diameter. The responsivity of samples (4), (3), (45), and (35) with 100-μm-diameter mesa at 1550 nm is 0.244, 0.239, 0.524, and 0.445 A/W, respectively. The high responsivity of 0.71 A/W at 1310 nm and 0.524 A/W at 1550 nm of our wafer-bonded Ge/Si p-i-n photodiode can be comparable with that of the epitaxial one.

Fig. 12(c) shows the responsivity of the devices illuminated by laser with different wavelengths. The responsivity of the four samples decreases with the increase in the wavelength. For samples (4) and (3), when the wavelength increases to 1630 nm, only ~0.02 A/W of the responsivity is achieved. This indicates that 1630 nm is close to the absorption edge of samples (4) and (3). This may be due to the 0.2%–0.3% in-plane compression strain in the exfoliated Ge film. For samples (45) and (35), the responsivity of ~0.11 A/W at 1630 nm is achieved. This value is one order of magnitude larger than that of samples (4) and (3). This is due to the bandgap narrowing induced by the in-plane tensile strain [41], [42]. This indicates that the wafer-bonded Ge/Si p-i-n photodiode can be used for optical communication in all wavelength division multiplexing bands, including the *L*-band and entire *C*-band.

IV. Conclusion

The layer exfoliation method is used for the fabrication of Si-based Ge film, which is very different from the epitaxial growth method. The exfoliated Ge film is suggested to contain low-density TDs ($<10^5$ cm^{-2}). The rms of the exfoliated Ge decreases from 17.5 to 0.131 nm after CMP and the bonded interface is demonstrated to be near-bubble-free. The TDs at Ge/Si interface can be eliminated at low temperature, leading to the high quality of the exfoliated Ge film. However, after postannealing at 500 °C, the TD density increases, leading to the worsening of the device performance. After pulse laser annealing, the junction depth of ~110 nm and the doping concentration of $>10^{19}$ cm^{-2} are achieved at room temperature. Low DCD of 5.97 mA/cm^2 and low ideality factor of 1.19 is obtained for the wafer-bonded Ge/Si p-i-n photodiode. The in-plane compression strain in exfoliated Ge film turns into tensile strain after postannealing, leading to the increase of the diode responsivity. The absorption edge of the postannealed Ge/Si photodiode expands to over 1630 nm due to the narrowing of the Ge bandgap induced by the tensile strain. Overall, the wafer bonding and smart cut technique are feasible for the fabrication of high-performance Si-based Ge photodiode at a very low temperature.

References

[1] Y. Kang *et al.*, "Monolithic germanium/silicon avalanche photodiodes with 340 GHz gain–bandwidth product," *Nature Photon.*, vol. 3, no. 1, pp. 59–63, Dec. 2009.
[2] P. Chaisakul *et al.*, "Integrated germanium optical interconnects on silicon substrates," *Nature Photon.*, vol. 8, no. 6, pp. 482–488, May 2014.
[3] J. Michel, J. Liu, and L. C. Kimerling, "High-performance Ge-on-Si photodetectors," *Nature Photon.*, vol. 4, pp. 527–534, Jul. 2010.
[4] L. Vivien *et al.*, "Zero-bias 40Gbit/s germanium waveguide photodetector on silicon," *Opt. Express*, vol. 20, no. 2, pp. 1096–1101, Jan. 2012.

[5] Z. Huang *et al.*, "21-GHz-bandwidth germanium-on-silicon photodiode using thin SiGe buffer layers," *IEEE J. Sel. Topics Quantum Electron.*, vol. 12, no. 6, pp. 1539–1544, Nov./Dec. 2006.
[6] C. T. DeRose *et al.*, "Ultra compact 45 GHz CMOS compatible Germanium waveguide photodiode with low dark current," *Opt. Express*, vol. 19, no. 25, pp. 24897–24904, Dec. 2011.
[7] W. S. Zaoui *et al.*, "Frequency response and bandwidth enhancement in Ge/Si avalanche photodiodes with over 840 GHz gain-bandwidth-product," *Opt. Express*, vol. 17, no. 15, pp. 12641–12649, Jul. 2009.
[8] S. Lischke *et al.*, "High bandwidth, high responsivity waveguide-coupled germanium p-i-n photodiode," *Opt. Express*, vol. 17, no. 23, pp. 27213–27220, Oct. 2015.
[9] E. Kasper, M. Kittler, M. Oehme, and T. Arguirov, "Germanium tin: Silicon photonics toward the mid-infrared," *Photon. Res.*, vol. 1, no. 2, pp. 69–76, Aug. 2013.
[10] J. Liu *et al.*, "Tensile strained Ge *p-i-n* photodetectors on Si platform for C and L band telecommunications," *Appl. Phys. Lett.*, vol. 87, no. 1, p. 011110, Jul. 2005.
[11] L. Colace, G. Masini, G. Assanto, H.-C. Luan, K. Wada, and L. C. Kimerling, "Efficient high-speed near-infrared Ge photodetectors integrated on Si substrates," *Appl. Phys. Lett.*, vol. 76, no. 10, pp. 1231–1233, Feb. 2000.
[12] H. Zang *et al.*, "Dark-current suppression in metal–germanium–metal photodetectors through dopant-segregation in NiGe—Schottky barrier," *IEEE Electron Device Lett.*, vol. 29, no. 2, pp. 161–164, Feb. 2008.
[13] J. L. Liu, S. Tong, Y. H. Luo, J. Wan, and K. L. Wang, "High-quality Ge films on Si substrates using Sb surfactant-mediated graded SiGe buffers," *Appl. Phys. Lett.*, vol. 79, no. 21, pp. 3431–3433, Sep. 2001.
[14] G. Zhou *et al.*, "Impacts of doping on epitaxial germanium thin film quality and Si-Ge interdiffusion," *Opt. Mater. Express*, vol. 8, no. 5, pp. 1117–1131, May 2018.
[15] H.-C. Luan *et al.*, "High-quality Ge epilayers on Si with low threading-dislocation densities," *Appl. Phys. Lett.*, vol. 75, no. 19, pp. 2909–2911, Sep. 1999.
[16] S. Ke *et al.*, "Voltage sharing effect and interface state calculation of a wafer-bonding Ge/Si avalanche photodiode with an interfacial GeO_2 insulator layer," *Opt. Express*, vol. 24, no. 3, pp. 1943–1952, Feb. 2016.
[17] J. R. Weber, A. Janotti, P. Rinke, and C. G. Van de Walle, "Dangling-bond defects and hydrogen passivation in germanium," *Appl. Phys. Lett.*, vol. 91, no. 14, p. 142101, Oct. 2007.
[18] Z. Liu *et al.*, "48 GHz high-performance Ge-on-SOI photodetector with zero-bias 40 Gbps grown by selective epitaxial growth," *J. Lightw. Technol.*, vol. 35, no. 24, pp. 5306–5310, Dec. 15, 2017.
[19] S. Huang *et al.*, "Depth-dependent etch pit density in Ge epilayer on Si substrate with a self-patterned Ge coalescence island template," *Thin Solid Films*, vol. 520, no. 6, pp. 2307–2310, Jan. 2012.
[20] C. Chen, C. Li, S. Huang, Y. Zheng, H. Lai, and S. Chen, "Epitaxial growth of germanium on silicon for light emitters," *Int. J. Photoenergy*, vol. 2012, Aug. 2012, Art. no. 768605.
[21] M. T. Currie, S. B. Samavedam, T. A. Langdo, C. W. Leitz, and E. A. Fitzgerald, "Controlling threading dislocation densities in Ge on Si using graded SiGe layers and chemical-mechanical polishing," *Appl. Phys. Lett.*, vol. 72, no. 14, pp. 1718–1720, Jul. 1998.
[22] J. Oh *et al.*, "Interdigitated Ge p-i-n photodetectors fabricated on a Si substrate using graded SiGe buffer layers," *IEEE J. Quantum Electron.*, vol. 38, no. 9, pp. 1238–1241, Sep. 2002.
[23] Q. Li, S. M. Han, S. R. J. Brueck, S. Hersee, Y.-B. Jiang, and H. Xu, "Selective growth of Ge on Si(100) through vias of SiO_2 nanotemplate using solid source molecular beam epitaxy," *Appl. Phys. Lett.*, vol. 83, no. 24, pp. 5032–5034, Dec. 2003.
[24] J.-S. Park, J. Bai, M. Curtin, B. Adekore, M. Carroll, and A. Lochtefeld, "Defect reduction of selective Ge epitaxy in trenches on Si(001) substrates using aspect ratio trapping," *Appl. Phys. Lett.*, vol. 90, no. 5, p. 052113, Feb. 2007.
[25] T. H. Loh *et al.*, "Selective epitaxial germanium on silicon-on-insulator high speed photodetectors using low-temperature ultrathin $Si_{0.8}Ge_{0.2}$ buffer," *Appl. Phys. Lett.*, vol. 91, no. 7, p. 073503, Aug. 2007.
[26] M. Steglich *et al.*, "Ge-on-Si photodiode with black silicon boosted responsivity," *Appl. Phys. Lett.*, vol. 107, no. 5, p. 051103, Aug. 2015.
[27] M. Schmid *et al.*, "Franz–Keldysh effect of germanium-on-silicon p-i-n diodes within a wide temperature range," *Thin Solid Films*, vol. 525, pp. 110–114, Dec. 2012.
[28] Y. Lin *et al.*, "High-efficiency normal-incidence vertical *p-i-n* photodetectors on a germanium-on-insulator platform," *Photon. Res.*, vol. 5, no. 6, p. 46, Dec. 2018.
[29] C.-Y. Yu, C.-Y. Lee, C.-H. Lin, and C. W. Liu, "Low-temperature fabrication and characterization of Ge-on-insulator structures," *Appl. Phys. Lett.*, vol. 89, no. 10, p. 101913, Sep. 2006.
[30] I. P. Ferain, K. Y. Byun, C. A. Colinge, S. Brightup, and M. S. Goorsky, "Low temperature exfoliation process in hydrogen-implanted germanium layers," *J. Appl. Phys.*, vol. 107, no. 5, p. 054315, Mar. 2010.
[31] X. Yu, J. Kang, R. Zhang, M. Takenaka, and S. Takagi, "Characterization of ultrathin-body Germanium-on-insulator (GeOI) structures and MOSFETs on flipped Smart-Cut GeOI substrates," *Solid-State Electron.*, vol. 115, pp. 120–125, Jan. 2016.
[32] Y. Ruan *et al.*, "Impacts of thermal annealing on hydrogen-implanted germanium and germanium-on-insulator substrates," *J. Electrochem. Soc.*, vol. 158, no. 11, pp. H1125–H1128, Jan. 2011.
[33] F. Gity *et al.*, "Characterization of germanium/silicon *p-n* junction fabricated by low temperature direct wafer bonding and layer exfoliation," *Appl. Phys. Lett.*, vol. 100, no. 9, p. 092102, Feb. 2012.
[34] A. M. Kiefer, D. M. Paskiewicz, A. M. Clausen, W. R. Buchwald, R. A. Soref, and M. G. Lagally, "Si/Ge junctions formed by nanomembrane bonding," *ACS Nano*, vol. 5, no. 2, pp. 1179–1189, Jan. 2011.
[35] K. H. Lee, A. Jandl, Y. H. Tan, E. A. Fitzgerald, and C. S. Tan, "Growth and characterization of germanium epitaxial film on silicon (001) with germane precursor in metal organic chemical vapour deposition (MOCVD) chamber," *AIP Adv.*, vol. 3, no. 9, p. 092123, Sep. 2013.
[36] Y. H. Tan and C. S. Tan, "Growth and characterization of germanium epitaxial film on silicon (001) using reduced pressure chemical vapor deposition," *Thin Solid Films*, vol. 520, no. 7, pp. 2711–2716, Jan. 2012.
[37] S. Ke *et al.*, "Low-temperature oxide-free silicon and germanium wafer bonding based on a sputtered amorphous Ge," *Appl. Phys. Lett.*, vol. 112, no. 4, p. 041601, Jan. 2018.
[38] S. Ke *et al.*, "Interface characteristics and electrical transport of Ge/Si heterojunction fabricated by low-temperature wafer bonding," *J. Phys. D, Appl. Phys.*, vol. 51, no. 26, p. 265306, May 2018.
[39] C. Miclaus and M. S. Goorsky, "Strain evolution in hydrogen-implanted silicon," *J. Phys. D, Appl. Phys.*, vol. 36, no. 10A, pp. A177–A180, Apr. 2003.
[40] K. E. Junge *et al.*, "Dielectric response of thick low dislocation-density Ge epilayers grown on (001) Si," *Appl. Phys. Lett.*, vol. 69, no. 26, pp. 4084–4086, Oct. 1996.
[41] J. Liu *et al.*, "High-performance, tensile-strained Ge *p-i-n* photodetectors on a Si platform," *Appl. Phys. Lett.*, vol. 87, no. 10, p. 103501, Aug. 2005.
[42] J. R. Jain, A. Hryciw, T. M. Baer, D. A. B. Miller, M. L. Brongersma, and R. T. Howe, "A micromachining-based technology for enhancing germanium light emission via tensile strain," *Nature Photon.*, vol. 6, no. 6, pp. 398–405, May 2012.

Authors' photographs and biographies not available at the time of publication.